

SCIENCE

MAS

WANG, X

Author

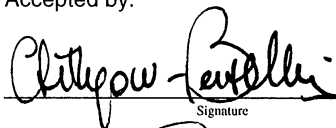
Xin Wang

Title

Present-day Three Dimensional
Temperature Distribution From a
Mantle Flow Model

submitted in partial fulfillment
of the requirements for the degree of
Master of Science in Geology
Department of Geological Sciences
The University of Michigan

Accepted by:


Signature

Carolina Lithgow-Bertelloni

5/21/08

Name

Date

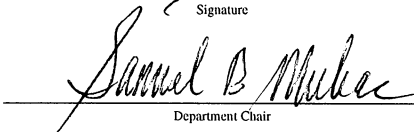

Signature

Lars Stixrude

5/22/08

Name

Date


Department Chair

Samuel Mukasa

8/4/08

Name

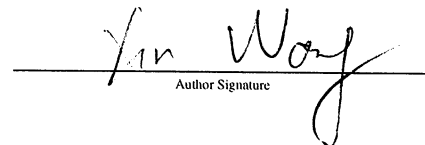
Date

I hereby grant the University of Michigan, its heirs and assigns, the non-exclusive right to reproduce and distribute single copies of my thesis, in whole or in part, in any format. I represent and warrant to the University of Michigan that the thesis is an original work, does not infringe or violate any rights of others, and that I make these grants as the sole owner of the rights to my thesis. I understand that I will not receive royalties for any reproduction of this thesis.

Permission granted.

Permission granted to copy after: _____
Date

Permission declined.


Author Signature

Tables of Contents

Lists of Tables and Figures	2
Abstract	3
1. Intruction	4
2. Models and Methods	7
2.1. Mantle flow model	7
2.2. Thermal Diffusion Equations	9
2.3. Finite Element Model	10
2.3.1. Finite Element Package ABAQUS	10
2.3.2. Two-Dimensional Oceanic Lithosphere Cooling Model..	11
2.3.3. Three-Dimensional Global Lithosphere Model	13
2.3.4. Three-Dimensional Global Mantle Model	14
3. Results and Discussion	16
References	19

List of Tables and Figures

Table 1	21
Figure 1	22
Figure 2	23
Figure 3	24
Figure 4	25
Figure 5	26
Figure 6	27
Figure 7	28
Figure 8	29
Figure 9	30
Figure 10	31
Figure 11	32

Abstract

In an attempt to understand the global temperature distribution in the mantle and its consequences for Earth structure we construct a model for the instantaneous temperature field of the mantle, assuming downwelling slabs to be the most important source of density heterogeneity and temperature variations. We neglect the contributions due to active upwellings. We use a model for the history of subduction derived from tectonic reconstructions and compute the 3-D velocity field for an incompressible Newtonian fluid. We solve the advection-diffusion equation in steady state for a spherical shell using the finite element package ABAQUS. We choose 3000 K temperature boundary condition at the core-mantle boundary. At the top, up to a depth of 100 km we constrain velocities to be plate velocities and derive the temperature boundary condition by solving the advection-diffusion equation for lithospheric cooling. The vertical resolution in the mantle below 100 km is on the order of 145 km in the mantle except for the bottom-most 300 km. The horizontal resolution is $\sim 5 \times 5^\circ$. We recover the half-space cooling behavior in the lithosphere and not surprisingly, the 3-D variations in the entire mantle are dominated by the presence of slabs in regions of long-lived subduction. We speculate on the effects on topography at the 410 and 660 km seismic discontinuities.

1. INTRODUCTION

Knowing the three-dimensional temperature structure and distribution in the mantle can help us gain a better understanding of Earth's interior, and has long been a goal in mantle studies. Lateral variations in temperature drive convective currents through their effect on density and also affect other physical properties, such as the elastic modulus that control wave speeds. Therefore, studying the 3-D temperature distribution of the mantle can lend insight into mantle dynamics, mineral physics and seismology.

The one-dimensional temperature profile of the mantle (the geotherm) has been studied extensively combining, petrological and mineral physics evidence [e.g. Jeanloz and Morris, 1986; Stacey, 1995]. In the lithosphere, the temperature is determined largely by conduction, modified by in situ heat production in the crust. In the mantle, the temperature gradient is principally the result of adiabatic compressibility, which we can compute from knowledge of mineral physics properties, such as the Grüneisen parameter. Figure 1 shows a possible geothermal gradient profile of the mantle [Brown and Mussett, 1981]. In the crust, the continental temperature gradient is shallower than the one for the oceans because the abundance of radioactive element is higher in continents. In the convective mantle part, the

temperature gradient is much shallower than the one above, and it cannot greatly exceed the adiabat. At the base of the mantle, the temperature gradient in a thin layer is again controlled by conduction. The temperature at the base of the mantle must be continuous with that in the core across the core-mantle boundary and is constrained by knowledge of the freezing point of iron alloys. The thin layers at the top and bottom are referred to as thermal boundary layers, which are commonly found in thermal convection systems. In the presence of layered convection we would expect another thermal boundary layer within the mantle, but evidence for this is scant. In this study, one of our goals is to study reasonable deviations from the geotherm.

The main goal of our work is to predict the three-dimensional instantaneous temperature distribution of the mantle. Since there is no way to observe the mantle temperature directly, the lateral temperature heterogeneity is often studied by some indirect ways, usually by comparing seismological observations to the results of mineral physics experiments or theory. Realistic numerical mantle convection simulations may also provide bounds on the lateral temperature structure of the mantle. However, this remains a distant goal, given the approximations in flow parameters and

physical properties, as well as tectonic history for most mantle convection simulations (Tackley, 2002; Bunge, 2005).

Here, we take a different approach rooted firmly in previous work (e.g. Lithgow-Bertelloni and Richards, 1998). First, we compute the instantaneous flow from a density heterogeneity model of the mantle based on the history of subduction. With these velocities, we solve the advection-diffusion equation in steady state to compute the 3-D instantaneous temperature distribution throughout the mantle. We analyze and discuss the results to show that our numerical models are consistent with our prediction.

2. Models and Methods

2.1 Mantle Flow Model

From the history of subduction derived from tectonic reconstructions, a density flow model can be constructed to drive viscous flow (Ricard et al., 1993; Lithgow-Bertelloni and Richards, 1998). For a prescribed density field, ignoring self-gravitation, the flow in an incompressible Newtonian fluid is governed by the equations for conservation of mass,

$$\nabla \cdot v = 0 \quad (1)$$

conservation of momentum

$$0 = \nabla \cdot \tau + f \quad (2)$$

and the constitutive relation for Newtonian creep.

$$\tau = -pI + 2\eta\dot{\epsilon} \quad (3)$$

where v is the velocity, p is the non-hydrostatic pressure, I is the identity matrix, η is the viscosity, $\dot{\epsilon}$ is the strain rate tensor, τ is the stress tensor, and $f = \delta\rho g$ is the body force, with $\delta\rho$ is the lateral density contrast and g is the gravitational acceleration. By substituting the constitutive relation into the conservation of momentum equation with the incompressibility condition, we obtain the Stokes equation for steady state viscous flow

$$\nabla p - \eta\nabla^2 v = f \quad (4).$$

To separate the vertical and horizontal components, velocity (v_r, v_θ, v_ϕ) and stresses ($\tau_{rr}, \tau_{r\theta}$, and $\tau_{r\phi}$) are represented with spherical harmonic expansions, with azimuthal and colatitudinal derivatives of the spherical harmonic function, which is defined with the associated Legendre polynomials. Substituting the expansions for velocity and stress into (1)-(3) we reduce the problem to a set of six coupled, first-order ordinary differential equations. By specifying six boundary values, which are no-slip at the surface and free slip at the core-mantle boundary, the equations are solved analytically via propagator matrices [Hager and O'Connell, 1979], and we can obtain stresses and velocities at any point in the interior. Here the density increasing with depth is not considered because we don't include compressibility.

2.2 Thermal Diffusion Equation

The heat transfer equation is defined as

$$\frac{\partial T}{\partial t} = \frac{k}{\rho C_p} \nabla^2 T + \frac{A}{\rho C_p} \quad (5)$$

where T is the temperature field, κ is the thermal diffusivity, which is $\frac{k}{\rho C_p}$,

k is the thermal conductivity, ρ is the density and C_p is the specific heat capacity at constant pressure, and A is the heat generation rate. If we

consider the motion of material, we need to add the effect of the motion of the material through the region where the temperature varies with depth.

Equation (5) becomes

$$\frac{\partial T}{\partial t} = \kappa \nabla^2 T + \frac{A}{\rho C_p} - \vec{v} \cdot \nabla T \quad (6)$$

Where \vec{v} is the three-dimensional velocity of material, and the term $\vec{v} \cdot \nabla T$ is the advection-transfer term. In the special situation when there is no heat generation, Equation (6) becomes

$$\frac{\partial T}{\partial t} = \kappa \nabla^2 T - \vec{v} \cdot \nabla T \quad (7)$$

This is the thermal diffusion equation with heat advection-transfer. For a steady-state situation when there is no change in temperature with time, Equation (7) becomes

$$0 = \kappa \nabla^2 T - \vec{v} \cdot \nabla T \quad (8)$$

This is a second-order partial differential equation, and we can solve Equation (8) to get the three-dimensional instantaneous temperature field, provided we already know the velocity field. The mantle flow model described above can provide the advection-transfer velocity \vec{v} . Numerical solutions to this equation were solved with a commercial finite element package.

2.3 Finite Element Model

2.3.1 Finite Element Package ABAQUS

The finite element method (FEM), also called the finite element analysis (FEA) is used for finding approximate numerical solutions to field problems, usually described by partial differential equations (PDE). FEM was first developed to solve complex elasticity, structural analysis problems in civil engineering and aeronautical engineering in 1940s. Since then, FEM has been developed rapidly, and it has found wide use in many science and engineering fields. Geoscientists also use FEM to solve problems in earth science, such as heat transfer, stress and strain, crust deformation, mantle convection, etc.

There are many finite element software packages (both free and proprietary) developed by companies and institutions. ABAQUS is a commercial software package for finite element analysis developed by SIMULIA, a brand of Dassault Systemes S.A. ABAQUS is widely used in automotive, aerospace, and industrial product industries, as well as in academic and research institutions due to the wide material modeling capability and strong heat transfer solvers. We use ABAQUS to solve our three-dimensional mantle model to get the instantaneous temperature field.

2.3.2 Two-Dimensional Oceanic Lithosphere Cooling Model

To avoid the numerical problems caused by big range of values and parameters, geodynamicists usually use non-dimensional analysis in studying geodynamics problems. In order to study how to non-dimensionalize the scale and how ABAQUS solves the heat transfer problem, we have tried some two-dimensional models to simulate the oceanic lithosphere cooling in ABAQUS.

In the half-space cooling model, the analytical thickness of oceanic lithosphere can be calculated from (Turcotte and Schubert, 1985),

$$\frac{T - T_0}{T_1 - T_0} = \operatorname{erf}\left(\frac{y}{2\sqrt{\kappa x/u}}\right) \quad (9)$$

where T_0 is the surface temperature, T_1 is the temperature beneath the plate, y is the thickness of the oceanic lithosphere, κ is the thermal diffusivity, x is the distance from the mid ocean ridge, and u is the plate spreading velocity.

We constructed a two-dimensional model with 150km in depth, and 1000km in distance with a spreading velocity 1cm/year , so that the oldest lithosphere is 100 million years old. In the dimensional analysis model, thermal conductivity k is $3\text{W}/(\text{m}\cdot\text{K})$, density ρ is $3000\text{kg}/\text{m}^3$, and specific heat C_p is $1000\text{J}/(\text{kg}\cdot\text{K})$. Plate spreading velocity v is $1\text{cm}/\text{yr} = 3.17 \times 10^{-10}\text{m}/\text{s}$, surface temperature T_0 is 300K , the isothermal temperature beneath plates T_1

is $1600K$, and the mid-ocean-ridge temperature is also set to be $T_1 = 1600K$. We run this model in a time period of $100Myr$, and reproduce the results of the analytical solution from (9) [Figure 2].

Having accurately reproduced the analytical system, we developed an intuition for the proper scaling of velocity for our 3-D models. The longest length distance $1000km$ is set to be 1, so the depth is $150/1000 = 0.15$, and the spreading velocity is set to be

$$\bar{v}^* = \frac{v}{v_r} = \frac{v}{\kappa/l} = v \times \frac{10^6}{10^{-6}} = v \times 10^{12} = 3.17 \times 10^2 \quad (10)$$

Non-dimensional parameters: \bar{k}^* , \bar{C}_p^* , and $\bar{\rho}^*$ are set to be 1. Isothermal temperature \bar{T}_1^* is 1, and the surface temperature \bar{T}_0^* is $0.1875 = 300/1600$. After running this model for the proper corresponding time period ($100Myr$), we properly reproduced the analytical solution [Figure 3].

In our two-dimensional model, both dimensional and non-dimensional results from ABAQUS are close to the analytical solution given by (9), which gives us confidence that we can solve this kind of heat transfer problem with ABAQUS. From this two-dimensional model, we also figure out the right scaling method to convert the three-dimensional model from dimensional to non-dimensional.

2.3.3 Three-Dimensional Global Lithosphere Model

First we construct a global lithosphere model with a depth of 150km. We use ABAQUS to solve Equation (8) with the plate velocities from the topmost layer of the subduction history. In this model, the lithosphere is divided into 15 layers with thickness of 10km, and each layer has the same velocity field, in which the vertical components are very small compared to the horizontal components [Figure 4]. Each layer has 2352 heat transfer elements (5×5 degree) with convection/diffusion control, which means there are 2354 nodes at each depth. All the mid-ocean-ridge nodes and subduction slab nodes were picked to give proper boundary conditions [Figure 5]. All the mid-ocean-ridge nodes and the bottom nodes at depth of 150km are given a temperature of 1600K, and the surface nodes are given a temperature of 300K. We also give a linear increasing temperature to the slab nodes, 300K at surface and 1600K at the bottom. Then we non-dimensionalize this model (\bar{k}^* , \bar{c}_p^* , $\bar{\rho}^*$, \bar{T}^* , \bar{l}^*) and run this in a steady state analysis with an input of mass flow rate \bar{v}^* for each node. This mass flow rate comes from the subduction history model. We get the temperature distribution of the lithosphere, which looks reasonable with the mid-ocean-ridge and subduction slabs [Figure 6]. The heat flow at the surface is shown in Figure

7. We can find the heat flow at the mid-ocean ridge is obvious higher than other place.

2.3.4 Three-Dimensional Global Mantle Model

We construct the mantle model from 100km to 2890km (core-mantle boundary) with the same type of finite element and the same number of nodes for each layer [Figure 8]. The whole mantle was divided into 28 layers with thickness of 145km except for the top most layer and the lowermost 10 layers with a thickness of 30km each [Table 1]. The mantle flow model is an incompressible fluid model, so it can't simulate the temperature increase due to adiabatic compressibility. The adiabatic temperature should be added back to the simulated results when we want to get the geothermal gradient of the mantle. The adiabatic temperature we choose is shown in [Table 1] and is computed from a self-consistent thermodynamic model of a pyrolitic mantle (Xu et al., 2008). We nondimensionalize this model (\bar{k}^* , \bar{C}_p^* , $\bar{\rho}^*$, \bar{T}^* , \bar{l}^*) with the experience from scaling the two-dimensional oceanic lithosphere cooling model. Boundary conditions at the top (100km) were the results from the global lithosphere model after subtracting the adiabatic temperature and nondimensionalizing [Figure 8c], as well as the boundary condition at the core mantle boundary was set to be 0.25 (400K after subtracting the

adiabatic temperature, and 0.25 after nondimensionlizing). We run this model in a steady state analysis with an input of mass flow rate \bar{v}^* for each node [Figure 9] to get the instantaneous temperature field.

3. Results and Discussion

We obtain the instantaneous temperature of each node in each layer of the three-dimensional mantle model from ABAQUS. After dimensionalizing and adding back the adiabatic temperature, results of several layers are shown in Figure 10. Our model doesn't consider active upwellings, either large-scale or plumes, so downwelling slabs control the flow and the temperature. Upwellings result from return flow from the slabs. The results confirm our expectations. We can see the regions with downwelling subduction slabs have considerably lower temperature. The regions with return upwelling flow have higher temperatures (eg. 500 degrees higher than slabs at the depth of 652.5km). Not surprisingly, the hottest regions are farthest away from the slabs, due to advection and conduction. In other words, regions far away from slabs are cooled less than those next to them. Our mantle distribution results represent the effect of our mantle flow model successfully.

We also calculated the average temperature of every layer and combined the results from both the lithosphere model and the mantle model to compute the geotherm with depth [Figure 11]. The geothermal gradient in the lithosphere part is nearly linear, but it is not as the same as the computed adiabat at greater depths. One possible reason is that we are missing heat

generation of radioactive elements in the lithosphere and mantle. From previous research, the heat generation of radioactive elements is at least 47% of the surface heat flow [Fowler, 2005]. Although the abundance of these elements in the crust is richer than it in the mantle, the contribution of mantle is still greater due to the large volume of the mantle. In our model, we don't account explicitly for this heat generation effect on the adiabat, although we do account for it indirectly. Our mantle density heterogeneity model assumes that only the top thermal boundary layer is important in generating buoyancy. This is the case for a mantle that is primarily internally heated, so that much of the buoyancy generating capacity goes into building the top boundary layer. Nonetheless, others have suggested that internal heating also results in subadiabatic temperature profiles (Jeanloz and Morris, 1987; Bunge et al., 2001), which we do not capture. Deviations in our model may also be caused by the absence of direct active upwellings (large scale or plumes).

It is also possible that an adiabat does not properly capture the geotherm of the mantle, where subduction is prevalent. The 1600 K adiabat is that typical of a normal mantle, not an average mantle cooled by slab mass fractions as high as 30% of the total volume in the transition zone. This is clear in our results, where besides a deeper lithosphere (because of a half-

space cooling solution) we have a cooler transition zone, where slabs may pond due to phase transitions and a viscosity increase between upper and lower mantle (Tackley et al., 1993).

It is clear from our maps in Figure 9 that the transition zone is dominated by the slab signal and this decreases with depth, with their presence felt as deep as 2000 km depth. The preponderance of a slab signal in the transition zone suggests that in the Western Pacific and Southeast Asia we should find a thicker transition zone and in the Eastern Pacific and Northern Europe a thinner transition zone. This is in good general agreement with seismological studies of topography on the 410 and 660 km discontinuities (e.g. Lawrence and Shearer, 2006).

In order to get more detailed temperature distribution and structure, future work should include: heat generation by radioactive elements, active upwellings, more reasonable boundary conditions (increasing the number of nodes and having more complicated temperature distribution at both the top and the core mantle boundary).

Reference

- Brown, G.C. & Mussett, A.E., 1981. *The inaccessible earth*. George Allen & Unwin. London.
- Bunge, H.P., 2005. Low plume excess temperature and high core heat flux inferred from non-adiabatic geotherms in internally heated mantle circulation models. *Physics of the earth and planetary interiors*. 153: 3-10.
- Bunge, H.P., Ricard, Y. & Matas, J., 2001. Non-adiabaticity in mantle convection. *Geophysical research letters*. 28: 879-882.
- Deschamps, F. & Trampert, J., 2003. Mantle tomography and its relation to temperature and composition. *Physics of the earth and planetary interior*. 140:277-291.
- Dziewonski, A.M. & Anderson, D.L., 1981. Preliminary reference earth model. *Physics of the earth and planetary interiors*. 25: 297-356.
- Fowler, C.M.R., 2005. *The solid earth*. Cambridge university press.
- Hager, B.H. & Oconnell, R.J., 1979. Kinematic models of large-scale flow in the earth's mantle. *Journal of geophysical research*. 84: 1031-1048.
- Jeanloz, R. & Morris, S., 1987. Is the mantle geotherm subadiabatic. *Geophysical research letters*. 14: 335-338.
- Lawrence, J.F. & Shearer, P.M., 2006. A global study of transition zone thickness using receiver function. *Journal of geophysical research-solid earth*. 111: B06307.
- Lithgow-Bertelloni, C. & Richards, 1998. M.A. The dynamics of Cenozoic and Mesozoic plate motions. *Reviews of geophysics*. 36: 27-78.
- Jeanloz, R. & Morris, S., 1986. Temperature distribution in the crust and mantle. *Ann. Rev. Earth Planet. Sci*. 14: 377-415.

- Ricard, Y., Richards, M.A. & Lithgow-Bertelloni, C., 1993. A geodynamic model of mantle density heterogeneity. *Journal of geophysical research-solid earth*. 98: 21895-21909.
- Stacey, F.D., 1995. Theory of thermal and elastic properties of the lower mantle and core. *Physics of the earth and planetary interiors*. 89: 219-245.
- Tackley, P.J. & Xie, S.X., 2002. Isotopic evolution of the mantle in numerical models of mantle convection and plate tectonics. *Geochimica et cosmochimica acta*. 66: A759-A759.
- Tackley, P.J., Stevenson, D.J. & Glatzmaier, G.A., 1993. Effects of an endothermic phase-transition at 670 km depth in a spherical model of convection in the earth's mantle. *Nature*. 361: 699-704.
- Turcotte, D.L. & Schubert, G., 1985. *Geodynamics*. Cambridge university press.
- Van den Berg, A.P., Rainey, E.S.G. & Yuen, D.A., 2005. The combined influences of variable thermal conductivity, temperature- and pressure-dependent viscosity and core-mantle coupling. *Physics of the earth and planetary interiors*. 149: 259-278.
- Xu, W., Lithgow-Bertelloni, C. & Stixrude, L., 2008. The effect of bulk composition and temperature on mantle seismic structure. *Earth and planetary science letter*. Submitted.
- Zhong, S., 2006. Constraints on thermochemical convection of the mantle from plume heat flux, plume excess temperature, and upper mantle temperature. *Journal of geophysical research-solid earth*. 111: B04409.

Table 1 Depth and adiabat temperature

<i>No.</i>	<i>Depth (km)</i>	<i>Radius (km)</i>	<i>Adiabat Temperature T_0 (K)</i>
1	100	6271	1657.819
2	217.5	6153.5	1708.027
3	362.5	6008.5	1767.660
4	507.5	5863.5	1862.914
5	652.5	5718.5	1928.667
6	797.5	5573.5	1957.748
7	942.5	5428.5	2009.695
8	1087.5	5283.5	2059.085
9	1232.5	5138.5	2106.096
10	1377.5	4993.5	2151.027
11	1522.5	4848.5	2194.410
12	1667.5	4703.5	2236.175
13	1812.5	4558.5	2277.002
14	1957.5	4413.5	2315.982
15	2102.5	4268.5	2354.614
16	2247.5	4123.5	2391.765
17	2392.5	3978.5	2430.484
18	2537.5	3833.5	2486.451
19	2590	3781	2517.539
20	2620	3751	2532.046
21	2650	3721	2540.374
22	2680	3691	2548.649
23	2710	3661	2556.864
24	2740	3631	2565.011
25	2770	3601	2573.033
26	2800	3571	2581.312
27	2830	3541	2589.533
28	2860	3511	2597.689
29	2890	3481	3005.690

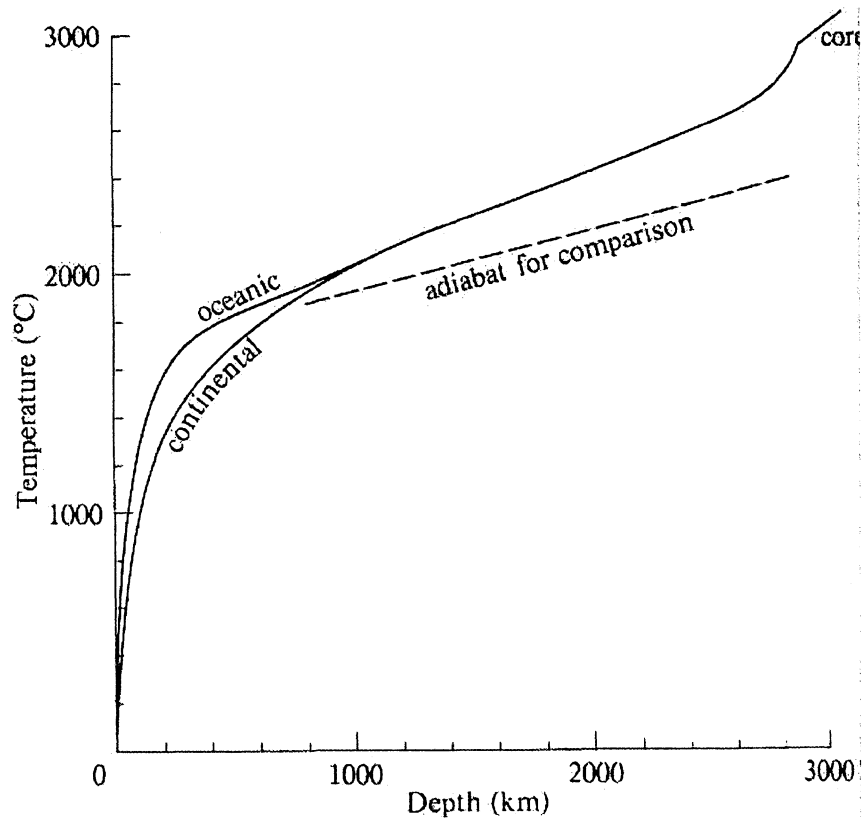


Figure 1 Possible temperature profiles in the mantle. [Brown, Mussett 1981]

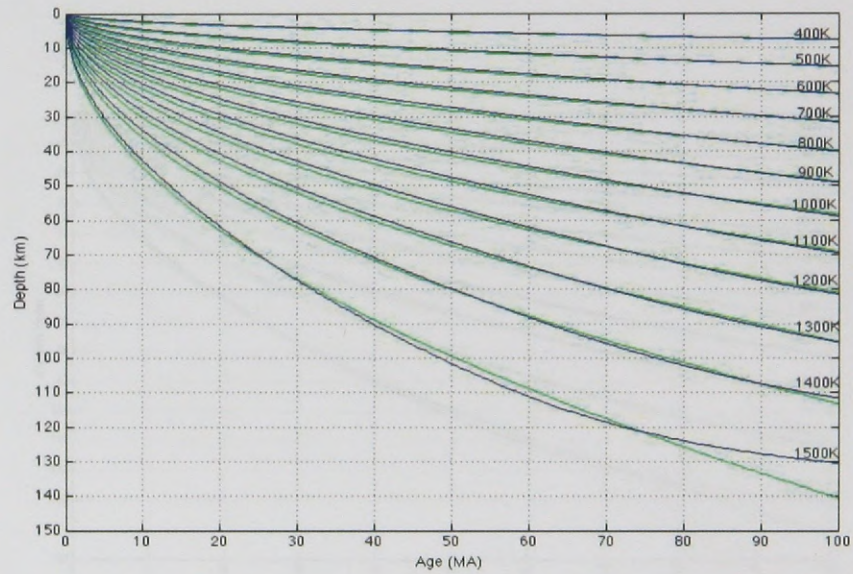


Figure 2 Two-dimensional oceanic lithosphere cooling. Isothermal lines show the results between our model (blue) and the analytical solutions (green).

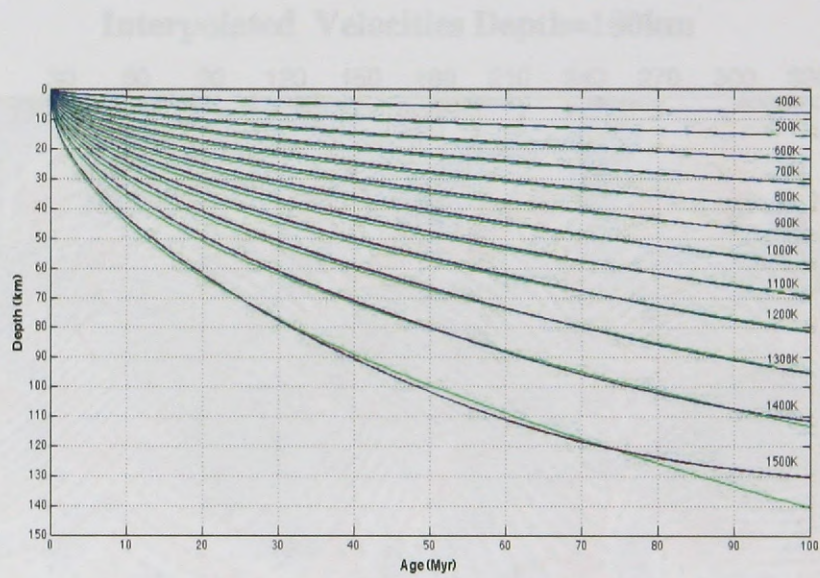


Figure 3 Dimensional and nondimensional oceanic lithosphere cooling.

Isothermal lines show the results of dimensional (blue), nondimensional (red), and analytical solution (green). Dimensional results and nondimensional results are almost the same.

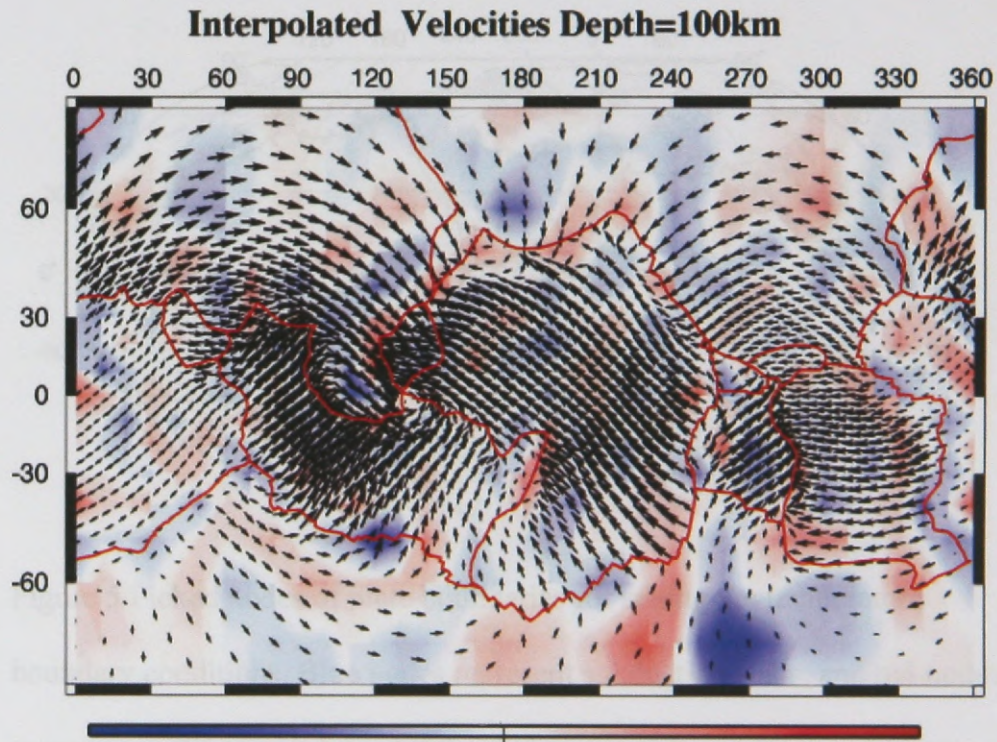


Figure 4 Nondimensional input velocity for the global lithosphere model.

The main part is horizontal component, and the vertical velocity is very small.

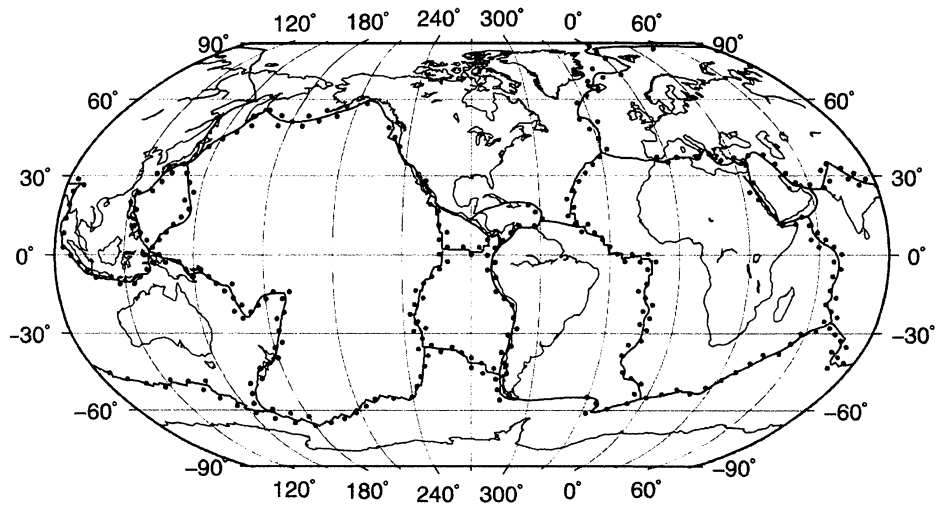


Figure 5 Picked nodes of plate boundaries for setting the temperature boundary conditions. Blue nodes represent subduction slabs, and red nodes represent mid-ocean-ridges. All the mid-ocean-ridge nodes are given an isothermal temperature of 1600K except the surface, the slab nodes are given a linear increasing temperature with depth (300K at the surface and 1600K at the bottom).

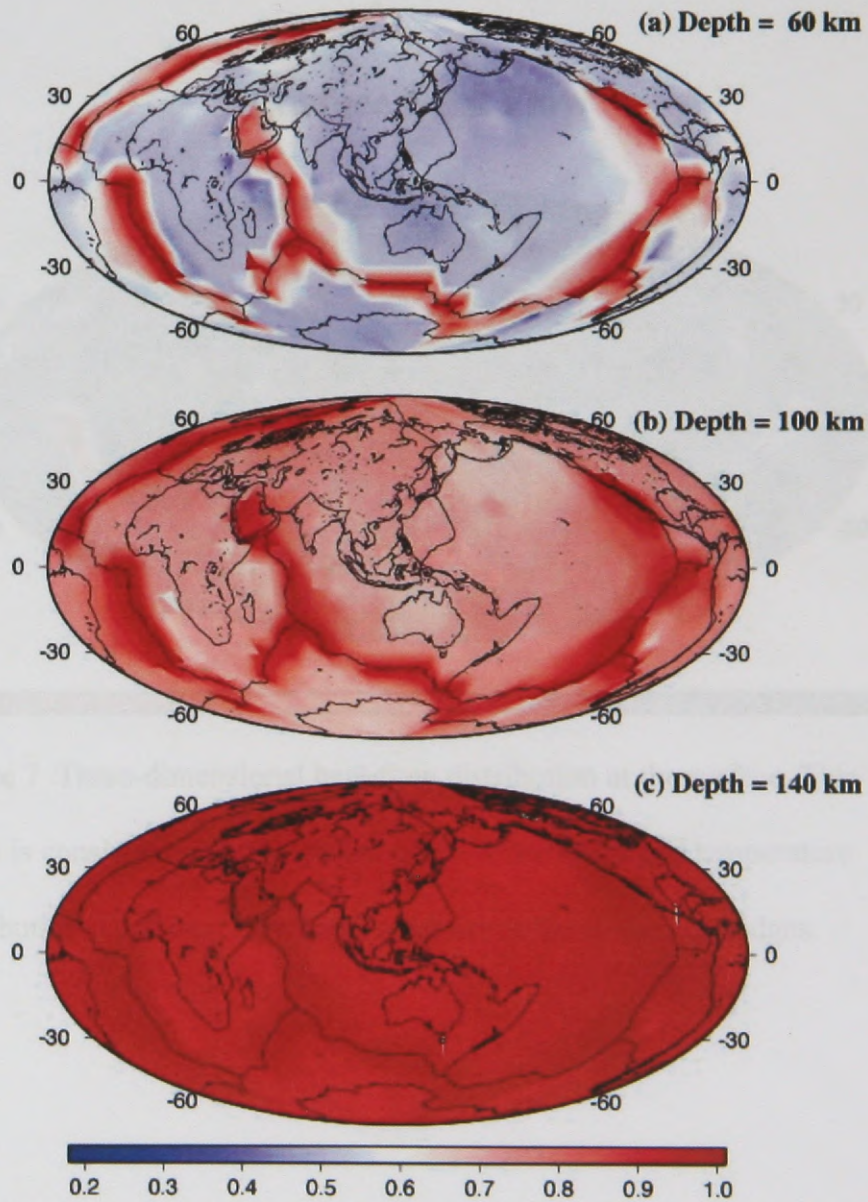


Figure 6 Three-dimensional temperature distribution of the lithosphere. (a) at depth of 60km, (b) at depth of 100km, (c) at depth of 140km. We chose (b) as our top boundary condition for the mantle model.

Surface Heat Flow

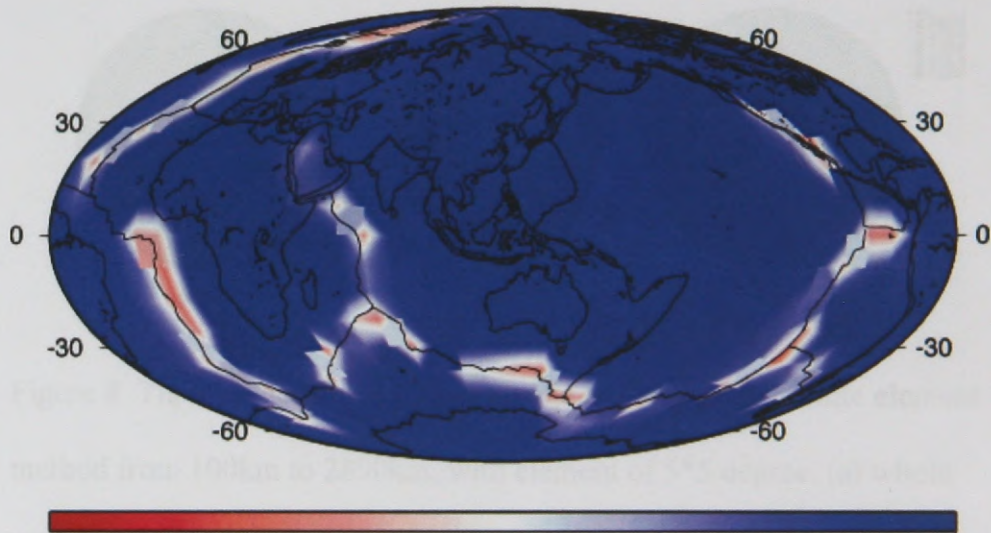


Figure 7 Three-dimensional heat flow distribution at the surface. This result is consistent with the picked nodes distribution and temperature distribution. High heat flow (red) areas are at the mid-ocean ridges.

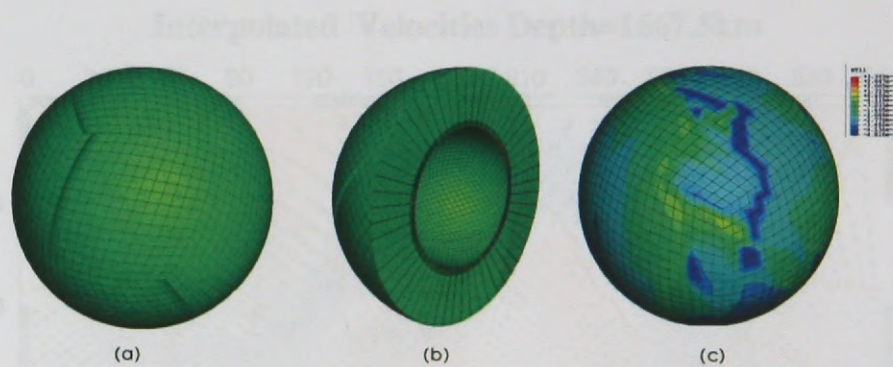


Figure 8 Three-dimensional global mantle model by using finite element method from 100km to 2890km, with element of 5*5 degree. (a) whole model, (b) cross section, (c) with the surface boundary condition of temperature at the depth of 100km.

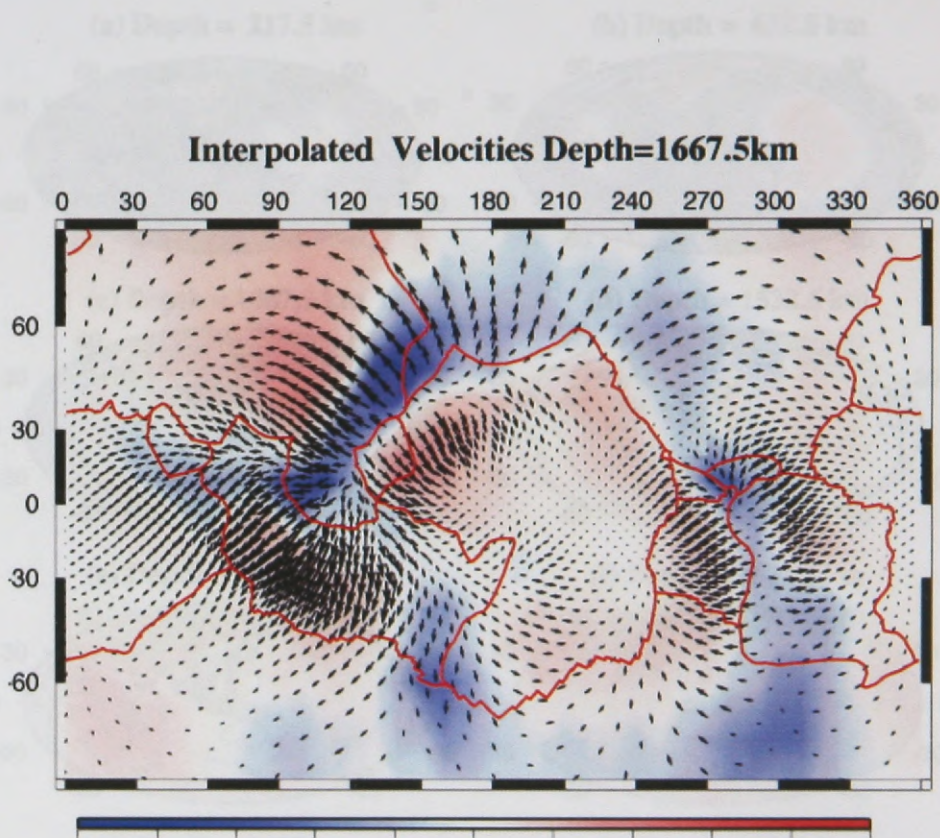


Figure 9 Nondimensional input velocity for the global mantle model at the depth of 1667.5km. Different from the lithosphere model, horizontal and vertical velocity are at the same order of magnitude.

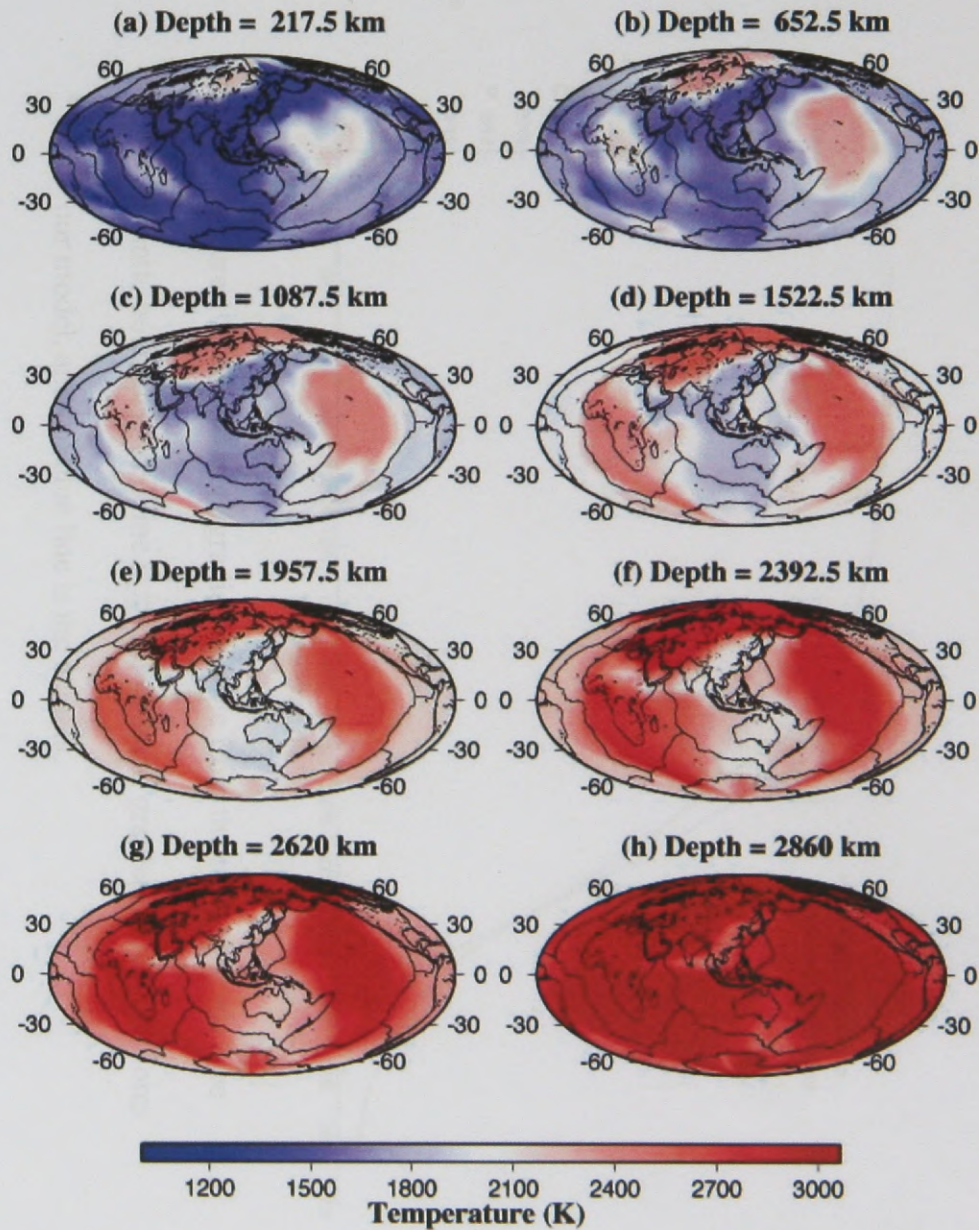


Figure 10 Three-dimensional mantle temperature distribution. (a)~(h) are the maps at different depth.

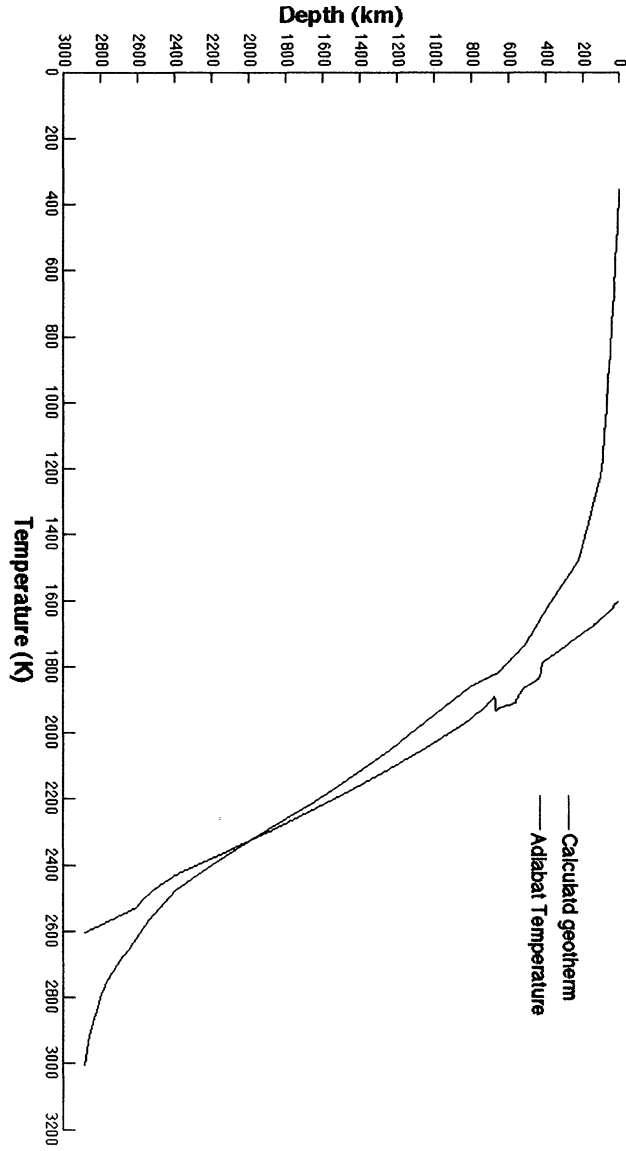


Figure 11 Temperature gradient profile from the surface to the core mantle boundary. Red line is the geothermal gradient calculated from our model, and the blue line is the adiabatic.

UNIVERSITY OF MICHIGAN



3 9015 07425 3504